IEEE Transactions on Microwave Theory and Techniques

In Situ Waveform Measurements Within Doherty Power Amplifier Under Operational Conditions

S. Probst
E. Denicke
B. Geck

Suggested Citation:
S. Probst, E. Denicke, and B. Geck. In Situ Waveform Measurements Within Doherty Power Amplifier Under Operational Conditions. *IEEE Transactions on Microwave Theory and Techniques*, 65(6):2192–2200, June 2017.

Digital Object Identifier (DOI): 10.1109/TMTT.2017.2651809

In Situ Waveform Measurements within a Doherty Power Amplifier under Operational Conditions

Steffen Probst, *Student Member, IEEE,* Eckhard Denicke, *Student Member, IEEE,* and Bernd Geck, *Member, IEEE*

***Abstract*—In this contribution a gallium nitride (GaN) based 1 GHz Doherty amplifier with in situ waveform measurement capability is presented. With this measurement approach the high frequency time domain voltages and currents can be measured directly within the circuit. Therefore, directional couplers are integrated into the output matching network of the carrier and the peak amplifier. In contrast to other measurement techniques for investigating amplifiers under laboratory conditions, with this approach a more in-depth investigation of realized power amplifiers can be carried out under operational conditions, e.g., for tuning. Especially, it is possible to characterize the interaction of the carrier and the peak amplifier. Hence, to the best knowledge of the authors the load modulation of a Doherty amplifier at the fundamental and the higher harmonics is measured for the first time.**

***Index Terms*—Doherty amplifier, high efficiency, in situ measurements, inverse class F, load modulation, non-linear systems, power amplifier, time domain measurements.**

I. Introduction

AMPLIFIER architectures are commonly complex circuits. Normally an amplifier is characterized by measuring input and output quantities and the direct current (DC) operation point. However, in some instances these quantities do not deliver enough knowledge to the developer about the grounds on which the performance of the power amplifier is based. Furthermore, knowledge about the high frequency voltages and currents (waveforms) is important at all levels of the design process, e.g., for the verification of the circuit design and its compliance with the system requirements [1], [2]. Thus, to get an understanding of the electrical quantities within the circuit of a power amplifier, in [3] a two-stage GaN amplifier is presented, in which the high frequency voltages in an interstage matching network are measured with a calibrated high impedance probe. Therein, the effect of the high frequency voltage waveform on the amplifier efficiency is investigated. However, for a more in-depth investigation of a power amplifier, the additional knowledge of the high frequency current is necessary.

Moreover, [4] proposes an approach for optimizing the efficiency of a silicon laterally diffused metal oxide semiconductor (Si-LDMOS) device under class F and inverse class F condition by measuring the high frequency voltages and currents using a sophisticated time domain load-pull system [5].

Furthermore, a variety of publications exists about device model extraction by means of calibrated measurement setups under laboratory conditions [6]–[8]. [8] presents an interesting setup, in which coupling networks are integrated into the matching networks of an amplifier in order to extract parameters for creating a non-linear model of the device under test (DUT). Regarding the topic of in-circuit measurements, in [9] a calibration procedure for power level on-wafer large-signal transistor characterization is described.

S. Probst, E. Denicke and B. Geck are with the Institute of Microwave and Wireless Systems, Leibniz Universität Hannover, Germany, 30167 Hannover (e-mail: probst@hft.uni-hannover.de).

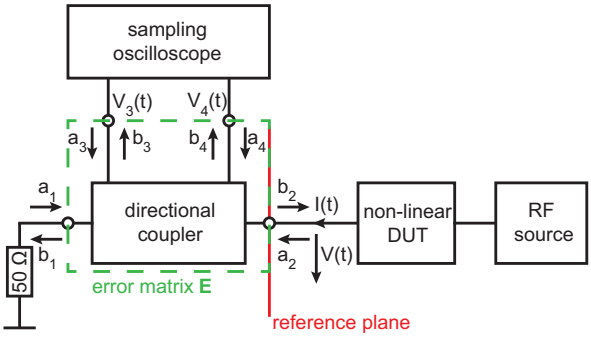

Fig. 1. Schematic of the in situ measurement setup.

The aforementioned publications are of particular interest in the predominant case of characterizing the non-linear behavior of a device (e.g., a transistor) under laboratory conditions. Furthermore, there are various publications on the field of de-embedding techniques with the aim of generating e.g., a transistor model [10]–[14]. By means of de-embedding techniques the transistor model provides knowledge to the designer about the intrinsic voltages and currents at the current source plane. Furthermore, a relationship between the intrinsic and the external voltages and currents in the package plane of the transistor model can be established.

In [15] calibrated measurements of the waveforms at the internal nodes of monolithic microwave integrated circuits (MMIC) with a large signal network analyzer (LSNA) and high impedance probes are presented.

Another interesting technique is the usage of high resolution microwave field probes [16]–[19]. The advantage of field probes is the use of an oscilloscope being basic measurement equipment in a test laboratory. However, using a probing setup is challenging with regard to the probe positioning accuracy. Additionally, the high resolution electrical field probe only detects the voltage waveforms within the circuit.

This work is focused on waveform measurements within a realized amplifier circuit under operational conditions in contrast to the characterization of solely an active device under laboratory conditions. The measurement approach is of great value e.g., for the verification of the design goals or for tuning

a circuit after fabrication.

In contrast to the forecited publications, in [20], [21] the high frequency voltages and additionally the currents are measured within the circuit, i.e., with a directional coupler embedded in the output matching network of a power amplifier under operational conditions. In this contribution the authors show, that with the additional benefit of knowing the waveforms it is possible and suitable to verify and optimize the design in terms of, e.g., the impedance conditions, the power and the efficiency. Therefore, a calibrated in situ measurement approach is presented for waveform measurements within a reference or calibration plane in a microstrip technology circuit.

For demonstration purposes, a more complex power amplifier structure in contrast to [21], a Doherty amplifier is used [22]. Doherty amplifiers have been published in several variants regarding technology, frequency and power range [23]–[30]. However, in these publications the load modulation, on which the efficiency enhancement for the back-off range is based, is not explicitly verified by measurements. With the in situ waveform measurements introduced in this contribution, the load modulation is measured at the fundamental and the higher harmonics, which – to the best of the authors' knowledge – has never been shown before. With the high frequency voltages and currents the interaction of the carrier and the peak amplifier is demonstrated.

This article is organized as follows. First, in Section II the operational principle of the in situ waveform measurement approach is introduced. Furthermore, the calibration procedure for a reference plane in a microstrip technology circuit is described. In order to verify the accuracy, setups for comparing the in situ approach to direct measurements with an oscilloscope or a vector network analyzer (VNA) are introduced. Subsequently in Section III, as an application of the in situ waveform measurement approach, a complex amplifier circuit, a 1 GHz Doherty amplifier, is used. This section describes the design, realization, tuning after initial commissioning and investigation of an inverted Doherty amplifier , based on two inverse class F power amplifiers as carrier and peak amplifiers. At last, this work is concluded in Section IV.

II. In Situ Waveform Measurements

Using the high frequency voltages $V\,(t)$ and currents $I\,(t)$ in time domain is a suitable approach for describing the behavior of non-linear radio frequency (RF) circuits. Fig. 1 shows the schematic of the measurement setup based on a sampling oscilloscope and a directional coupler. In this contribution the measurement setup is realized as a microstrip technology circuit with a reference plane set to a position on a microstrip line with a characteristic impedance of $Z_0 = 50\,\Omega$. The directional coupler separates the incident and scattered waves of the DUT. The coupled voltages $V_3\,(t)$ and $V_4\,(t)$ are measured in time domain with the sampling oscilloscope. Herein, the input reflection coefficient of the oscilloscope is assumed to be negligible, which was affirmed by measurements over the frequency range of $0.5\,\mathrm{GHz}$ to $6\,\mathrm{GHz}$.

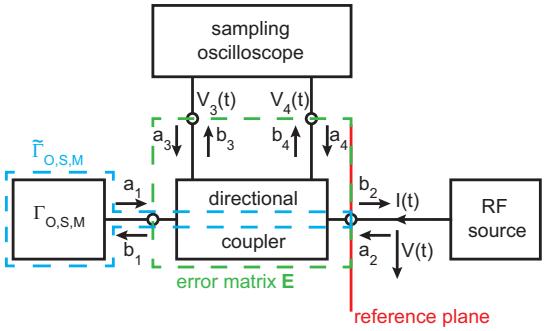

Fig. 2. Schematic of the in situ measurement setup for the OSM calibration.

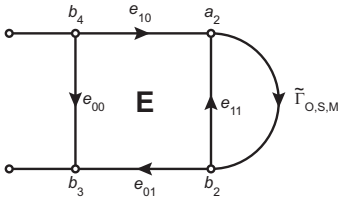

Fig. 3. Signal flow graph of the error matrix **E** connected to the standards $\Gamma_{\mathrm{O,S,M}}$.

A. Concept

To calculate $V\,(t)$ and $I\,(t)$ in the reference plane the measurement setup has to be calibrated taking into account the frequency response of the measurement setup (including the directional coupler and cables). In this context, a TOSM (Thru, Open, Short, Match) calibration procedure [5] is enhanced by using calibration standards pre-characterized via the TRL (Thru, Reflect, Line) method [31]. Therefore, the frequency of the RF source is swept to the distinct frequency points, i.e., to the fundamental frequency f_1 and to the considered higher harmonics (up to $6f_1$) (cp. Fig. 2 for the calibration setup). The four-port coupler can be defined by means of the four-port / two-port reduction [32] and thus can be described by a 2×2 error matrix **E** with coefficients e_{xy} for each frequency point, which are shown in Fig. 3. The relationship between the a_2- and b_2-waves in the calibration plane and the coupled waves b_3 and b_4 emerge from the signal flow graph of **E** (compare Fig. 3) as:

$$a_2 = e_{11}b_2 + e_{10}b_4\ , \tag{1}$$

$$b_2 = \frac{b_3 - e_{00}b_4}{e_{01}}\ . \tag{2}$$

For calculating the error coefficients three standards connected successively to port 1 of the coupler are required, e.g., Open ($\Gamma_{\mathrm{O}} \approx 1$), Short ($\Gamma_{\mathrm{S}} \approx -1$) and Match ($\Gamma_{\mathrm{M}} \approx 0$) (cp. Fig. 2). The effective reflection coefficients $\tilde{\Gamma}_{\mathrm{O,S,M}}$ of the standards in the reference plane (cp. Fig. 2) are pre-determined with a TRL calibrated VNA. From Fig. 3 the following equation in its three states can be derived:

$$\frac{b_{3,\mathrm{O,S,M}}}{b_{4,\mathrm{O,S,M}}} = e_{00} + \frac{e_{10}e_{01}\tilde{\Gamma}_{\mathrm{O,S,M}}}{1 - e_{11}\tilde{\Gamma}_{\mathrm{O,S,M}}}\ . \tag{3}$$

With these three measurements the error coefficients e_{00}, e_{11} and the product $e_{10}e_{01}$ are determined.

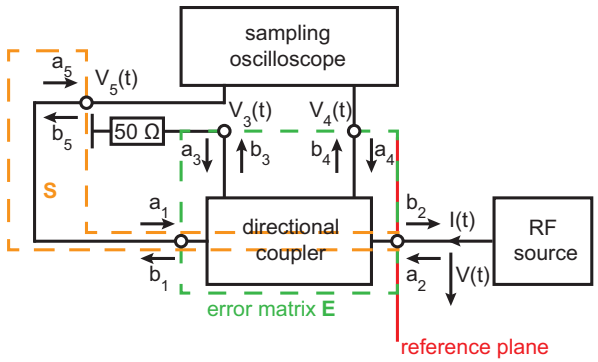

Fig. 4. Schematic of the in situ measurement setup for the thru calibration.

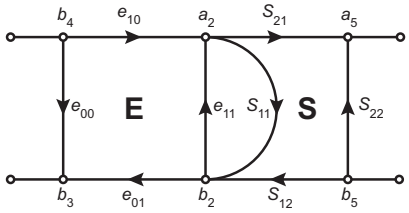

Fig. 5. Signal flow graph of the error matrices **E** and **S** for the thru calibration.

In addition, it is required to separate the product of the error coefficients $e_{10}e_{01}$, in order to calculate the a_2- and b_2-waves (cp. (1) and (2)). Therefore, a thru calibration to the reference plane is used. Fig. 4 exhibits the measurement setup for the thru calibration and Fig. 5 shows the accompanying signal flow graph with the error coefficients e_{xy} and the scattering coefficients S_{xy}. The scattering coefficients S_{xy} of the matrix **S**, which are pre-determined with a VNA, include a measurement cable and the microstrip line to the reference plane. Furthermore, the signal flow graph from Fig. 5 results in:

$$\frac{a_5}{b_4} = \frac{e_{10}S_{21}}{1 - e_{11}S_{11}} \ . \tag{4}$$

After the thru calibration all error coefficients are determined. The measured coupling voltages $V_3\,(t)$ and $V_4\,(t)$ (which in the calibration process are still mono-frequent for each frequency point) are transformed by the fast Fourier transformation into the frequency-domain quantities $V_3\,(f)$ and $V_4\,(f)$. The waves can be calculated as follows for a discrete frequency point f_n:

$$b_3\,(f_n) = |V_3\,(f_n)| \exp\left[j\angle\left(V_3\,(f_n)\right)\right] / \sqrt{Z_0} \ , \tag{5}$$

$$b_4\,(f_n) = |V_4\,(f_n)| \exp\left[j\angle\left(V_4\,(f_n)\right)\right] / \sqrt{Z_0} \ . \tag{6}$$

In (5) and (6) exp corresponds to the exponential function with the Euler's number as base. Furthermore, the complex voltage $V\,(f_n)$ and current $I\,(f_n)$ can be determined considering (1), (2), (5) and (6):

$$V\,(f_n) = \left(a_2\,(f_n) + b_2\,(f_n)\right) \cdot \sqrt{Z_0} \ , \tag{7}$$

$$I\,(f_n) = \left(a_2\,(f_n) - b_2\,(f_n)\right) / \sqrt{Z_0} \ . \tag{8}$$

The high frequency voltage $V\,(t)$ and current $I\,(t)$ in the DUT's reference plane in time domain are determined with

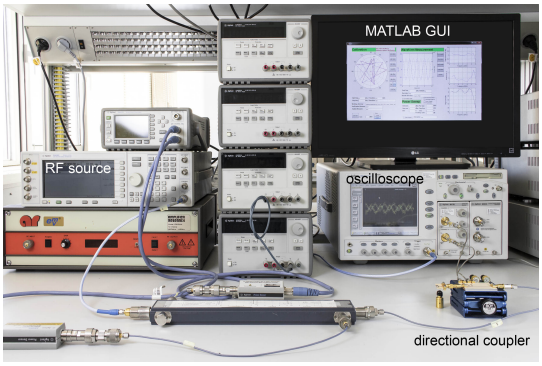

Fig. 6. Measurement setup for the in situ waveform measurement approach.

(7) and (8) for each frequency point as a Fourier series:

$$V\,(t) = \sum_{n=1}^{N} |V\,(f_n)\,| \cdot \cos\left(2\pi n f_1 t + \angle\left(V\,(f_n)\right)\right) \ , \tag{9}$$

$$I\,(t) = \sum_{n=1}^{N} |I\,(f_n)\,| \cdot \cos\left(2\pi n f_1 t + \angle\left(I\,(f_n)\right)\right) \ . \tag{10}$$

In (9) and (10) N corresponds to the number of considered harmonics (herein up to $6f_1$). If a DC bias in the reference plane of an actual DUT exists, this offset of $V(t)$ and $I(t)$ has to be measured separately and has to be added to (9) and (10).

B. Proof of concept

To determine the accuracy of the in situ measurement approach a comparison between a direct measurement and the in situ measurement with the coupler is conducted. For the measurements the sampling oscilloscope Agilent 86100B with module 86117B is used (compare Fig. 6). As signal source the signal generator Agilent 4430C is utilized and synchronized to the oscilloscope. At first, the in situ determined impedance of a passive load in the reference plane is compared with a VNA (Rohde & Schwarz ZVA24) measurement. Furthermore, waveform and measured power are verified through direct measurements in comparison to the in situ measurement approach.

1) Impedance: As a reference the impedance in the calibration plane is directly measured with a TRL calibrated VNA and obtained from the in situ measurement approach with the directional coupler (cp. Fig. 7). The test board is identical to the one of the calibration setup. Therefore, a verification reflection termination Γ_{Verify} is connected to the coupler, which translates to the measured $\tilde{\Gamma}_{\text{verify}}$ in the reference plane and its impedance $Z_{\tilde{\Gamma}_{\text{verify}}}$. The results for the normalized impedance $Z_{\tilde{\Gamma}_{\text{verify}}}/Z_0$ are presented in Fig. 8. The comparison between both methods in a frequency range of 0.5 GHz to 6 GHz shows a good agreement. For a more detailed comparison the difference between both methods for magnitude and phase of $\tilde{\Gamma}_{\text{Verify}}$ is presented in Fig. 9.

2) Waveform: Furthermore, in order to exhibit the accuracy of the waveform measurement, a test circuit is used, which consists of two diodes, one connected in series to a microstrip line and the other one connected to ground (cp.

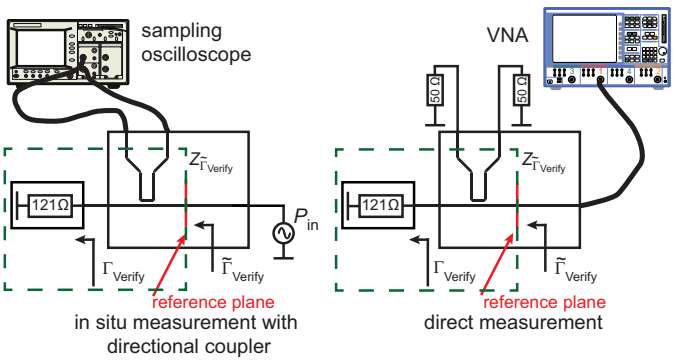

Fig. 7. Impedance measurement verification setups for the in situ measurement with directional coupler and sampling oscilloscope and for the direct measurement with the VNA.

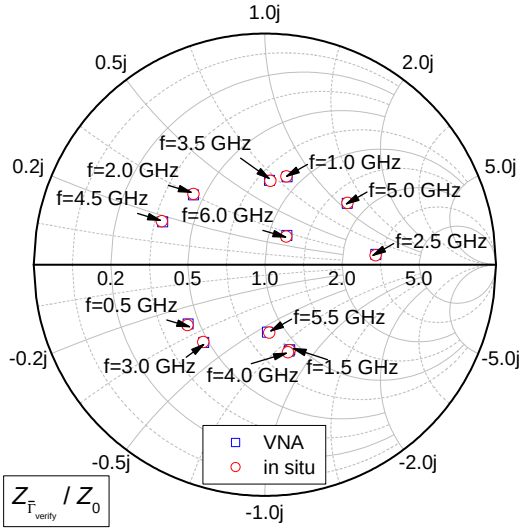

Fig. 8. Normalized measured impedance $Z_{\tilde{\Gamma}_{\text{Verify}}}/Z_0$.

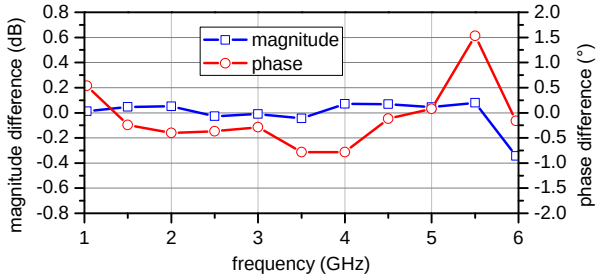

Fig. 9. Magnitude and phase difference between VNA and in situ measurement of $\tilde{\Gamma}_{\text{Verify}}$.

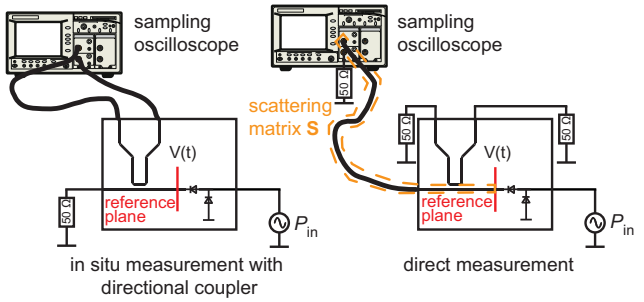

Fig. 10. Waveform measurement verification setups for the in situ measurement with directional coupler and for the direct measurement, both with the sampling oscilloscope.

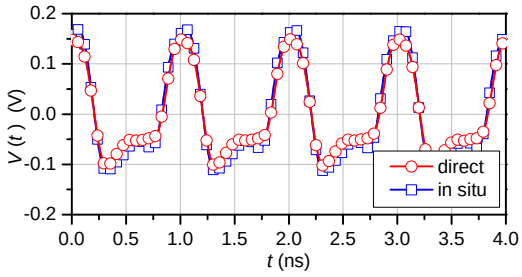

Fig. 11. Voltage waveform for the test circuit at $P_{\text{in}} = 6\,\text{dBm}$ and $f_1 = 1\,\text{GHz}$.

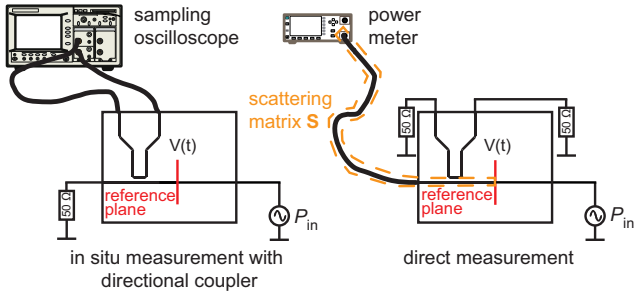

Fig. 12. Power measurement verification setups for the in situ measurement with directional coupler and for the direct measurement with a power meter.

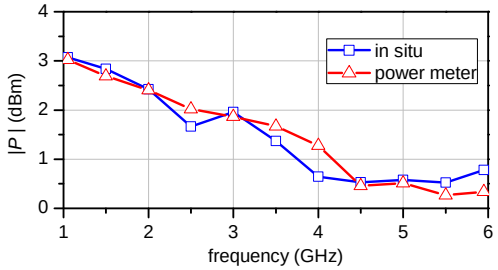

Fig. 13. Comparison of the power measured with the in situ approach and a power meter.

Fig. 10). At the left hand side of the circuit a directional coupler is embedded, which is an exact reproduction of the one on the calibration board. The RF source provides an available source power of $P_{\text{in}} = 6\,\text{dBm}$ with a frequency of $f_1 = 1\,\text{GHz}$. The resulting voltages $V(t)$ in the reference plane are calculated in MATLAB for the in situ measurement approach (cp. (9)) as well as for a direct measurement with the sampling oscilloscope directly connected to the test circuit (using the pre-characterized cable of the thru calibration for the correction of the reference plane by means of **S**). A comparison of the results in Fig. 11 shows a good agreement of both measurements. The diodes clip and attenuate the input signal. As a result of the non-linear behavior of the diodes the signal contains higher harmonics. Thus, Fig. 11 indicates the functionality of the in situ waveform measurement system for the fundamental frequency and the higher harmonics.

3) Power: Additionally, a comparison of the in situ determined power and the measurement result of a power meter

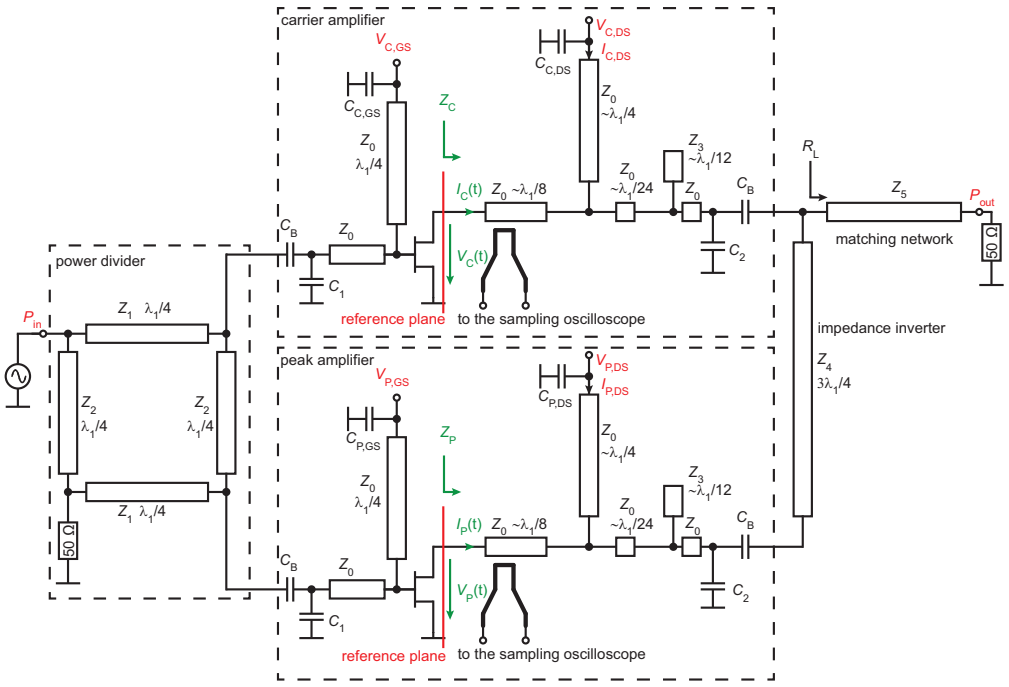

Fig. 14. Schematic of the developed 1 GHz inverted Doherty amplifier.

is made. Therefore, the calibration board, which consists of a microstrip line and the directional coupler, is used (cp. Fig. 4). The power meter is connected to the board with the pre-characterized cable of the thru calibration setup, whereas a correction to the reference plane is made using **S**. A continuous wave (CW) signal is used, which is swept in frequency from 1 GHz to 6 GHz. The power is calculated with the waveforms measured by the sampling oscilloscope and is compared to the results of the power meter (cp. Fig. 13). The measurements in this section demonstrated the functionality of the in situ approach. The slight deviations between in situ and comparison measurements might result from dynamic range issues due to the coupler design with its low coupling factor of $-35\,\mathrm{dB}$ at the fundamental frequency $f_1 = 1\,\mathrm{GHz}$ and of $-25\,\mathrm{dB}$ at $6f_1 = 6\,\mathrm{GHz}$. Another fact, that may contribute negatively to the measurement precision, could be the handling of the measurement setup in terms of movements of the cables after calibration. Additionally, small deviations between the couplers of the calibration board and of the DUT may exist due to the fabrication process.

In the next section the integration of the measurement approach into the output matching network of a power amplifier is described.

III. Application in a Doherty Power Amplifier

In this section initially a brief introduction to the theoretical behavior of a Doherty amplifier is given. Furthermore, the design and realization of an inverted Doherty amplifier with embedded in situ measurement approach is described, accompanied by measurement results.

A. Theory

The classical Doherty architecture according to [22] consists of two single amplifiers, the carrier and the peak amplifier, whereas the input signal is split with a power divider into both of them. At the output both amplifiers are connected over an impedance inverter to a common load. The performance of the Doherty amplifier can be divided into two parts, the low power and the high power range. In the low power range only the carrier amplifier is active, because the input signal of the peak amplifier is smaller than its threshold voltage, which is defined by the bias point. In the high power range both amplifiers are active. The efficiency of the Doherty amplifier is investigated, e.g., in [28], [33]. In the high power range the efficiency only varies by a small amount in dependence of the back-off, whereas a slight efficiency drop exists dependent on the load modulation of the carrier amplifier and the power ratio of the carrier and the peak amplifier [33]. The theoretical behavior of the amplifier load impedance over the normalized input voltage is shown, e.g., in [27]. The optimal load of the carrier amplifier decreases for increasing output power, because the peak amplifier begins to amplify. In this case, for maximal output power, both amplifiers have the same optimal load impedance. This load modulation of the carrier amplifier enhances the overall efficiency of the Doherty amplifier. In consequence, due to the interaction of the two amplifiers with their different optimal impedances for different back-off states, the knowledge of the impedances within the circuit (measurable with the proposed in situ approach) is of high significance for the developer.

B. Design and realization

Fig. 14 shows the schematic of the developed 1 GHz inverted Doherty amplifier, which was designed with Agilent

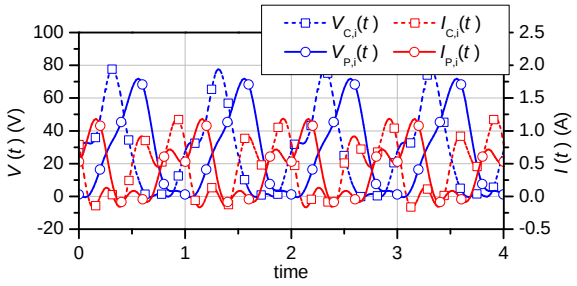

Fig. 15. Simulated intrinsic high frequency voltages ($V_{\mathrm{C,i}}(t), V_{\mathrm{P,i}}(t)$) and currents ($I_{\mathrm{C,i}}(t), I_{\mathrm{P,i}}(t)$) for the carrier and the peak amplifier for $P_{\mathrm{out,max}} = 42.2\,\mathrm{dBm}$.

Advanced Design System (ADS). To verify the performance of the amplifier the input and output powers (P_{in} and P_{out}) as well as the DC operating point ($V_{\mathrm{C,GS}}$, $V_{\mathrm{C,DS}}$, $I_{\mathrm{C,DS}}$, $V_{\mathrm{P,GS}}$, $V_{\mathrm{P,DS}}$ and $I_{\mathrm{P,DS}}$) are usually available for measurement with basic laboratory equipment (red colored quantities in Fig. 14). However, the load modulation effect of the Doherty amplifier and the waveforms of the time domain signals at the transistors can not be obtained from these quantities. To get a better understanding of the interaction of the carrier and the peak amplifier, directional couplers are integrated into the output matching network of both amplifiers. The coupling factor is dimensioned in order to minimize the influence on the circuit from the fundamental frequency f_1 up to the higher harmonics including $6f_1$. With the couplers it is possible to measure the high frequency voltages and currents in time domain in the reference plane at the package of the transistor ($V_{\mathrm{C}}(t)$, $I_{\mathrm{C}}(t)$, $V_{\mathrm{P}}(t)$ and $I_{\mathrm{P}}(t)$, green colored quantities in Fig. 14).

The carrier and the peak amplifier are designed as identical inverse class F amplifiers similar to the design proposed in [21]. The inverse class F operation mode (proper termination of all harmonics in the current source plane) was verified by evaluating the intrinsic voltages and currents of the manufacturer's large-signal model (cp. [34]). The waveforms are presented in Fig. 15. As a design restriction due to the couplers, the harmonic terminations are positioned behind the coupler in order to allow a reference plane at the transistor package. The coupler design regarding its characteristic impedance etc. should be customized regarding the requirements of the given device or matching network. The harmonic terminations within the output matching network are shown in Fig. 14. Due to the design of the chosen amplifiers with their impedance behavior an inverted Doherty amplifier architecture is used according to [25], [29]. Furthermore, the theoretical waveforms of an inverse class F amplifier can be found in [35].

In order to split the input signal for the carrier and the peak amplifier a branch line coupler with uneven power division was developed (cp. [36]). The uneven power division is beneficial for biasing the peak amplifier in the B/C operation point in order to deliver more power [37]. As impedance inverter a $3\lambda_1/4$-line is used. The load R_{L} of the Doherty amplifier is transformed with a simple matching network to the system impedance of $Z_0 = 50\,\Omega$.

Fig. 16 shows the realized inverted Doherty power amplifier with embedded directional couplers. The power amplifier is

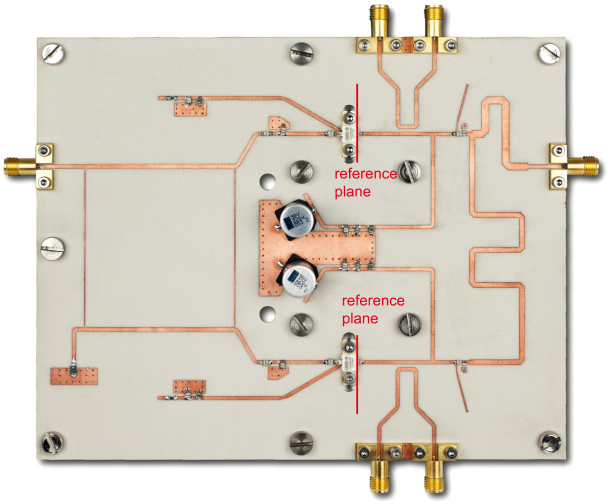

Fig. 16. Realized 1 GHz inverted Doherty amplifier.

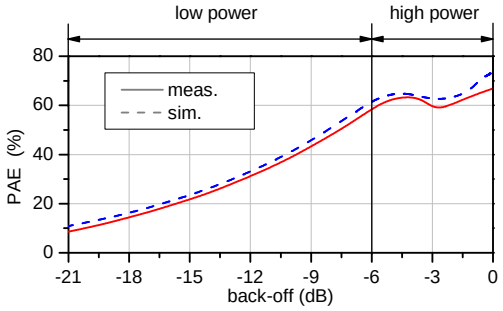

Fig. 17. Simulated and measured power added efficiency after the initial commissioning.

designed on a Rogers RO4003 substrate ($\varepsilon_{\mathrm{r}} = 3.55$, thickness $h = 508\,\mu\mathrm{m}$). The printed circuit board is mounted on an aluminium plate to ensure stability, proper heat dissipation and assembling of the transistors. The carrier and the peak amplifier both use a 10 Watt GaN high electron mobility transistor (HEMT) from Cree (CGH40010F). Based on experimental work, the gate bias voltage of the carrier amplifier is set to $V_{\mathrm{C,GS}} = -2.75\,\mathrm{V}$ and for the peak amplifier to $V_{\mathrm{P,GS}} = -3.40\,\mathrm{V}$. The DC supply for the drain bias voltage for both amplifiers is $V_{\mathrm{C,DS}} = V_{\mathrm{P,DS}} = 28\,\mathrm{V}$. The fundamental frequency is $f_1 = 1\,\mathrm{GHz}$.

C. Initial commissioning and tuning

For the first commissioning, the Doherty power amplifier was characterized in terms of the input and output quantities and the DC operation point. The power added efficiency (PAE) is obtained from the simulated and measured input and output power (P_{in} and P_{out}), which is depicted over the back-off range in Fig. 17. Obviously, the measured PAE is lower than the simulated one. However, with the knowledge of only the input and output quantities, it would be cumbersome to tune the efficiency of the amplifier, due to the fact that the efficiency depends on many design parameters, i.e., especially on the impedance terminations of all harmonics. Advantageously, by means of the in situ measurement approach it is possible to

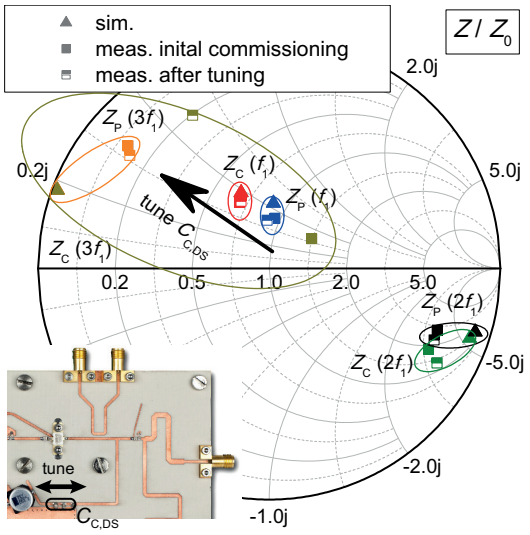

Fig. 18. Simulated and measured normalized impedance terminations at high power for f_1, $2f_1$ and $3f_1$ (0 dB back-off) after the initial commissioning and after the tuning process.

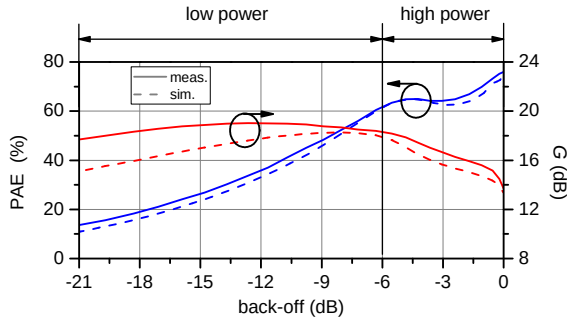

Fig. 19. Simulated and measured power added efficiency and gain after tuning.

verify the impedance terminations of the carrier and the peak amplifier.

Before the actual in situ measurement is conducted, the calibration procedure of the time domain waveform measurement setup is carried out with the described calibration board at the fundamental frequency and the higher harmonics (cp. Section II), after which the voltage and current waveforms are determined in the reference planes of the amplifiers. Additionally, with the measured waveforms the impedance terminations for both inverse class F amplifiers are calculated at the fundamental frequency and the higher harmonics. Fig. 18 shows the simulated and measured normalized impedance terminations of f_1, $2f_1$ and $3f_1$ at high power (0 dB back-off) for the carrier and the peak amplifier after initial commissioning. For the fundamental frequency and the second harmonic, the measurement results agree sufficiently with the simulation results in the reference plane at the package of the transistor. However, the measured third harmonic termination of the carrier amplifier deviates clearly from the simulation. Thus, this indicates that the carrier amplifier's matching network (cp. Fig 14) of the higher harmonics might be imperfect. Within the matching network the capacitance $C_{\mathrm{C,DS}}$ consists of three capacitors. The position of the capacitors is essential for the termination of the fundamental and the higher harmonics as seen from the current source plane [21]. Hence, a

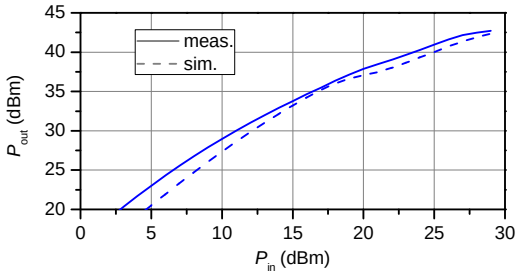

Fig. 20. Simulated and measured output power P_{out} after tuning.

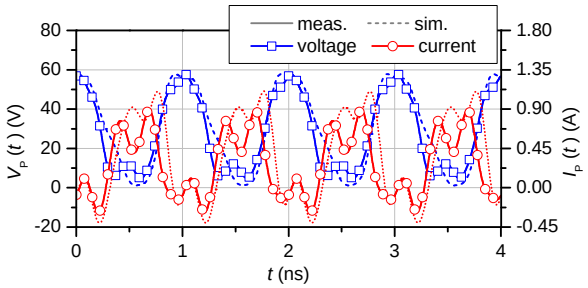

Fig. 21. Simulated and measured waveforms in the reference plane of the peak amplifier for $P_{\mathrm{out,max}} = 42.2\,\mathrm{dBm}$ after tuning.

deficient positioning of the capacitors due to the fabrication process and the manual placement may lead to a degraded performance. Thus, the capacitors were moved (cp. Fig. 18), while monitoring the impedance termination until a satisfying match between measurement and simulation was achieved. Consequently, the knowledge of the harmonic terminations assists the developer to tune the amplifier in order to meet the specifications and to match simulation and measurement.

After the tuning process, the harmonic terminations of the finalized inverted Doherty amplifier were measured once again. The results are depicted in Fig. 18. Obviously, the third harmonic termination of the carrier amplifier $Z_C(3f_1)$ is tuned to the range of the measured third harmonic termination of the peak amplifier $Z_P(3f_1)$. Furthermore, the gain G and the PAE are presented in Fig. 19. The PAE progression in dependence of the back-off indicates the functioning of the load modulation. Additionally, the output power P_{out} was measured and compared with the simulation (cp. Fig. 20).

Moreover, the in situ measurement of the high frequency voltages and currents enables a comfortable way to further investigate the interaction of both amplifiers in detail as shown in the following.

D. In situ measurement results of the finalized amplifier

Fig. 21 shows the simulated and measured high frequency voltage and current at the reference plane of the peak amplifier over time for the maximal output power $P_{\mathrm{out,max}} = 42.2\,\mathrm{dBm}$, which delivers further insight into the efficiency behavior of the transistor. This results can be used e.g., for calculating the de-embedded waveforms at the intrinsic sources [10]–[12], which might be valuable at higher frequencies.

The interaction of the carrier and the peak amplifier can be described by the fundamental high frequency voltages and

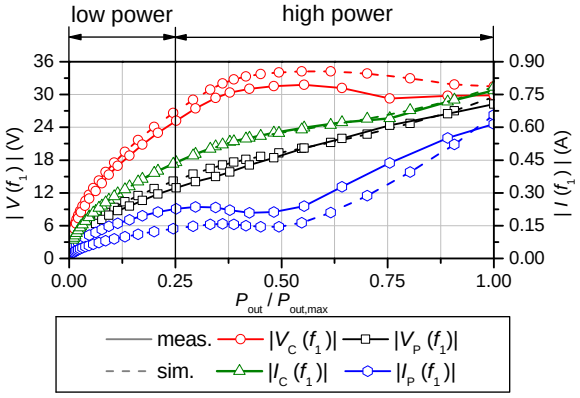

Fig. 22. Simulated and measured magnitudes of the voltages and currents at fundamental frequency f_1 for the carrier and the peak amplifier after tuning.

currents [25], [33]. Hence, Fig. 22 shows the relationship of the magnitude of the high frequency voltages ($|V_{\mathrm{C}}(f_1)|$, $|V_{\mathrm{P}}(f_1)|$) and currents ($|I_{\mathrm{C}}(f_1)|$, $|I_{\mathrm{P}}(f_1)|$) at f_1 in the reference plane of the carrier and the peak amplifier over the normalized output power $P_{\mathrm{out}}/P_{\mathrm{out,max}}$. In the high power range both amplifiers are active and the current of the carrier amplifier increases, while the voltage is approximately constant, which results in the high efficiency in this range. In general, a satisfying agreement between simulation and measurement exists. However, there is still some potential for improving the load modulation with help of the in situ measurements in a proceeding development process.

Furthermore, Fig. 23 shows the simulated and measured load modulation at the reference plane of the carrier and the peak amplifier for the inverted Doherty amplifier over the output power P_{out}. At the fundamental frequency f_1 the impedance $Z_C(f_1)$ as seen from the carrier amplifier is almost constant for low output power (LP), which corresponds to the operation of a single amplifier without load modulation. In the high output power range (HP) the impedances $Z_C(f_1)$ and $Z_P(f_1)$ of both amplifiers nearly converge to the same value. Thus, the function of the load modulation for this inverted Doherty amplifier is confirmed.

Fig. 23 additionally shows the impedance terminations for the second ($Z_C(2f_1)$, $Z_P(2f_1)$) and third ($Z_C(3f_1)$, $Z_P(3f_1)$) harmonic as seen from the carrier and the peak amplifier over the output power P_{out}. In theory, the second harmonic should be terminated as an Open in the current source plane, which is approximately satisfied here in the transistor package plane as well for $Z_C(2f_1)$ over the whole power range, whereas $Z_P(2f_1)$ is arbitrary in the low power range for the non-operational peak amplifier. In theory, the third harmonic should be terminated as a Short in the current source plane, which is approximately met here likewise in the package plane for the whole power range of both amplifiers ($Z_C(3f_1)$, $Z_P(3f_1)$). The peak amplifier shows a slightly more fluctuating behavior in its non-operational state as expected.

Obviously, the influence of the deficiently placed capacitors on the termination of the third harmonic has been fixed sufficiently.

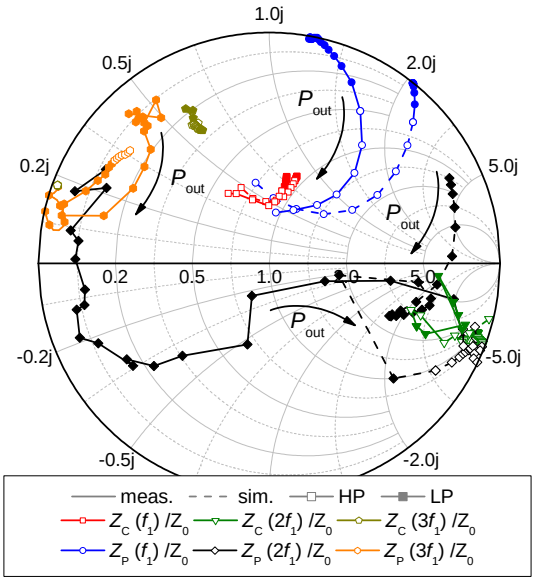

Fig. 23. Simulated and measured normalized impedance terminations during the load modulation for f_1, $2f_1$ and $3f_1$ after tuning.

IV. Conclusion

In this contribution a calibrated in situ waveform measurement approach is presented, which is embedded into the output matching networks of the carrier and the peak amplifiers of a 1 GHz inverted Doherty power amplifier. The in situ approach offers the chance to get further knowledge of the high frequency voltage and current waveforms within the circuit. With this knowledge, e.g., the power, impedance conditions and efficiency under operational conditions can be investigated in detail, e.g., for tuning. In situ measurements are of particular advantage for complex amplifier topologies, such as shown with the Doherty amplifier. The in situ approach is verified by various comparisons to other direct measurement methods with a sampling oscilloscope or a VNA. Future research may include enhancing the measurement approach by adapting a contactless measurement concept omitting circuit integrated couplers (cp. [38]). Furthermore, to the best knowledge of the authors, the load modulation of a Doherty power amplifier in conjunction with the interaction of its carrier and its peak amplifier is verified by measurements at the fundamental and the higher harmonics for the first time.

References

[1] P. Tasker, "RF Waveform Measurement and Engineering," in *Annual IEEE Compound Semiconductor Integrated Circuit Symposium*, Oct 2009, pp. 1–4.

[2] P. Tasker, "Practical Waveform Engineering," *IEEE Microwave Magazine*, vol. 10, no. 7, pp. 65–76, Dec 2009.

[3] A. Ramadan, T. Reveyrand, A. Martin, J.-M. Nebus, P. Bouysse, L. Lapierre, J.-F. Villemazet, and S. Forestier, "Two-Stage GaN HEMT Amplifier With Gate-Source Voltage Shaping for Efficiency Versus Bandwidth Enhancements," *IEEE Transactions on Microwave Theory and Techniques*, vol. 59, no. 3, pp. 699–706, Mar 2011.

[4] A. Sheikh, C. Roff, J. Benedikt, P. Tasker, B. Noori, J. Wood, and P. Aaen, "Peak Class F and Inverse Class F Drain Efficiencies Using Si LDMOS in a Limited Bandwidth Design," *IEEE Microwave and Wireless Components Letters*, vol. 19, no. 7, pp. 473–475, July 2009.

[5] J. Benedikt, R. Gaddi, P. Tasker, and M. Goss, "High-Power Time-Domain Measurement System with Active Harmonic Load-Pull for High-Efficiency Base-Station Amplifier Design," *IEEE Transactions on Microwave Theory and Techniques*, vol. 48, no. 12, pp. 2617–2624, Dec 2000.

[6] K. El-Akhdar, S. Ahmed, T. Reveyrand, G. Neveux, D. Barataud, and J. Nebus, "High Resolution Wideband Calibration Procedure for RF Time-Domain Measurement of Non-linear Devices," in *81st Microwave Measurement Conference (ARFTG)*, June 2013, pp. 1–4.

[7] K. El-Akhdar, G. Neveux, D. Barataud, and J. Nebus, "Calibrated Oscilloscopic System for RF Time-Domain Characterization of Non-linear Devices," in *13th Mediterranean Microwave Symposium (MMS)*, Sept 2013, pp. 1–4.

[8] M. Sipila, K. Lehtinen, and V. Porra, "High-Frequency Periodic Time-Domain Waveform Measurement System," *IEEE Transactions on Microwave Theory and Techniques*, vol. 36, no. 10, pp. 1397–1405, Oct 1988.

[9] A. Ferrero and U. Pisani, "An Improved Calibration Technique for On-Wafer Large-Signal Transistor Characterization," *IEEE Transactions on Instrumentation and Measurement*, vol. 42, no. 2, pp. 360–364, Apr 1993.

[10] G. Crupi and D. M. M.-P. Schreurs, *Microwave De-embedding: From Theory to Applications*, 1st ed. Elsevier, 2014.

[11] H. Jang, P. Roblin, and Z. Xie, "Model-Based Nonlinear Embedding for Power-Amplifier Design," *IEEE Transactions on Microwave Theory and Techniques*, vol. 62, no. 9, pp. 1986–2002, Sept 2014.

[12] A. Raffo, V. Vadala, G. Avolio, G. Bosi, A. Nalli, D. M. M.-P. Schreurs, and G. Vannini, "Linear Versus Nonlinear De-embedding: Experimental Investigation," in *81st Microwave Measurement Conference (ARFTG)*, June 2013, pp. 1–5.

[13] A. Raffo, F. Scappaviva, and G. Vannini, "A New Approach to Microwave Power Amplifier Design Based on the Experimental Characterization of the Intrinsic Electron-Device Load Line," *IEEE Transactions on Microwave Theory and Techniques*, vol. 57, no. 7, pp. 1743–1752, July 2009.

[14] A. Sheikh, C. Roff, J. Benedikt, P. Tasker, B. Noori, P. Aaen, and J. Wood, "Systematic Waveform Engineering Enabling High Efficiency Modes of Operation in Si LDMOS at both L-band and S-band Frequencies," in *IEEE MTT-S International Microwave Symposium*, June 2008, pp. 1143–1146.

[15] T. Reveyrand, A. Mallet, J. M. Nebus, and M. V. Bossche, "Calibrated Measurements of Waveforms at Internal Nodes of MMICs with a LSNA and High Impedance Probes," in *62nd Microwave Measurements Conference (ARFTG)*, Dec 2003, pp. 71–76.

[16] S. C. Cripps and A. Porch, "An Active, Non-intrusive, High Resolution Microwave Field Probe with Applications in High Power RF Device and Circuit Design," in *IEEE 11th Annual Wireless and Microwave Technology Conference (WAMICON)*, April 2010, pp. 1–4.

[17] N. Dehghan, S. Cripps, A. Porch, and J. Lees, "An Improved Electric Field Probe with Applications in High Efficiency PA Design and Diagnostics," in *81st Microwave Measurement Conference (ARFTG)*, June 2013, pp. 1–4.

[18] N. Dehghan, A. Porch, S. C. Cripps, and P. H. Aaen, "A Novel High Resolution E-Field Microscope System with Applications in HPA Diagnostics," in *78th Microwave Measurement Symposium (ARFTG)*, Dec 2011, pp. 1–3.

[19] N. Dehghan and S. C. Cripps, "A Novel In-Situ Calibration Technique for a High Resolution E-Field Probe," in *IEEE MTT-S International Microwave Symposium (IMS)*, May 2015, pp. 1–3.

[20] B. Pichler, N. Leder, and H. Arthaber, "Calibration Method for Coupler Based Time Domain Waveform Measurements," in *IEEE MTT-S International Workshop on integrated Nonlinear Microwave and Millimetre-wave Circuits, Taormina, Italy*, Oct 2015, pp. 1–3.

[21] S. Probst and B. Geck, "In Situ Waveform Measurement Approach with an Inverse Class F GaN Power Amplifier," in *IEEE MTT-S International Workshop on integrated Nonlinear Microwave and Millimetre-wave Circuits, Taormina, Italy*, Oct 2015, pp. 1–3.

[22] W. H. Doherty, "A New High Efficiency Power Amplifier for Modulated Waves," *Proceedings of the Institute of Radio Engineers*, vol. 24, no. 9, pp. 1163–1182, Sept 1936.

[23] A. Grebennikov and S. Bulja, "High-Efficiency Doherty Power Amplifiers: Historical Aspect and Modern Trends," *Proceedings of the IEEE*, vol. 100, no. 12, pp. 3190–3219, Dec 2012.

[24] D. McCarthy and T. Williams, "Applying Active Load-Pull in Doherty Power Amplifier," *Evaluation Engineering*, vol. 1, pp. 34–37, June 2011.

[25] G. Ahn, M.-S. Kim, H.-C. Park, S.-C. Jung, J.-h. Van, H. Cho, S.-W. Kwon, J.-H. Jeong, K.-H. Lim, J. Y. Kim, S. C. Song, C.-S. Park, and Y. Yang, "Design of a High-Efficiency and High-Power Inverted Doherty Amplifier," *IEEE Transactions on Microwave Theory and Techniques*, vol. 55, no. 6, pp. 1105–1111, June 2007.

[26] R. Darraji and F. Ghannouchi, "Digital Doherty Amplifier With Enhanced Efficiency and Extended Range," *IEEE Transactions on Microwave Theory and Techniques*, vol. 59, no. 11, pp. 2898–2909, Nov 2011.

[27] A. Mohamed, S. Boumaiza, and R. Mansour, "Electronically Tunable Doherty Power Amplifier for Multi-Mode Multi-Band Base Stations," *IEEE Transactions on Circuits and Systems I*, vol. 61, no. 4, pp. 1229–1240, April 2014.

[28] F. Raab, "Efficiency of Doherty RF Power-Amplifier Systems," *IEEE Transactions on Broadcasting*, vol. BC-33, no. 3, pp. 77–83, Sept 1987.

[29] S. Kwon, M. Kim, S. Jung, J. Jeong, K. Lim, J. Van, H. Cho, H. Kim, W. Nah, and Y. Yang, "Inverted-Load Network for High-Power Doherty Amplifier," *IEEE Microwave Magazine*, vol. 10, no. 1, pp. 93–98, February 2009.

[30] B. Kim, I. Kim, and J. Moon, "Advanced Doherty Architecture," *IEEE Microwave Magazine*, vol. 11, no. 5, pp. 72–86, Aug 2010.

[31] M. Hiebel, *Fundamentals of Vector Network Analysis*, 3rd ed. Rohde & Schwarz, 2008.

[32] S. A. Dyer, Ed., *Wiley Survey of Instrumentation and Measurement*. New York, NY, USA: Wiley, 2001.

[33] S. C. Cripps, *Advanced Technique in RF Power Amplifier Design*. Artech House, 2002.

[34] R. Pengelly, W. Pribble, and T. Smith, "Inverse Class-F Design Using Dynamic Loadline GaN HEMT Models to Help Designers Optimize PA Efficiency [Application Notes]," *IEEE Microwave Magazine*, vol. 15, no. 6, pp. 134–147, Sept 2014.

[35] A. Grebennikov and F. Sokal, *Switchmode RF and Microwave Power Amplifiers*, 2nd ed. Academic Press, 2012.

[36] H.-R. Ahn and I. Wolff, "Asymmetric Four-Port and Branch-Line Hybrids," *IEEE Transactions on Microwave Theory and Techniques*, vol. 48, no. 9, pp. 1585–1588, Sep 2000.

[37] R. S. Peggelly and S. M. Wood, "N-Way RF Power Amplifier Circuit with Increased Back-off Capabilitiy and Power Added Efficiency Using Unequal Input Power Devision," U.S. Patent US 6,737,922 B2, May 18, 2004.

[38] T. Zelder and B. Geck, "Contactless Scattering Parameter Measurements," *IEEE Microwave and Wireless Components Letters*, vol. 21, no. 9, pp. 504–506, Sept 2011.

Steffen Probst (S'15) was born in Seesen, Germany, in 1987. He received the Dipl.-Ing. degree in electrical and communication engineering from the Universität Kassel, Germany, in 2012 and the M.Sc. degree in electrical engineering from the Leibniz Universität Hannover, Germany, in 2014.

Since 2014, he has been a Research Assistant with the Institute of Microwave and Wireless Systems, Leibniz Universität Hannover.

His research interests include efficiency enhancement of power amplifiers and non-linear high frequency measurement techniques.

Mr. Probst received the 2014 Airbus Defence and Space Electronics ARGUS Award for his master thesis. He was also the recipient of Second Place of the GeMiC 2014 Student Design Competition.

Eckhard Denicke (S'09) was born in Hannover, Germany, in 1982. He received the Dipl.-Ing. degree in electrical engineering from the Leibniz Universität Hannover, Germany, in 2008.

Since then, he has been a Research Assistant with the Institute of Microwave and Wireless Systems, Leibniz Universität Hannover. His research interest is focused on RF identification (RFID) and multiple-input multiple-output (MIMO) systems. Further fields of research are microwave measurement techniques and radar applications, e.g., for industrial level gauging, including antenna design, as well as signal processing.

Mr. Denicke was the recipient of the 2008 EADS Defence Electronics ARGUS Award and the 2008 VDE Student Award for his diploma thesis. He was also the recipient of Third Place of the AMTA Symposium 2009 Student Paper Contest and the 2009 EEEfCOM Innovation Award as member of a research consortium for contributions on "Advances in Industrial Radar Level Measurements".

Bernd Geck (M'10) was born in Oldenburg, Germany, in 1959. He received the Dipl.-Ing. and Dr.-Ing. degrees in electrical engineering from the Leibniz Universität Hannover, Germany, in 1987 and 1997, respectively. From 1987 to 1992, he was a Research Assistant with the Institute of Radiofrequency and Microwave Engineering. In this time, he was involved in radio frequency network analyzer techniques.

From 1992 to 2010, he was Senior Engineer and since 2010, he is responsible for several lectures and research projects at the Institute of Radiofrequency and Wireless Systems. Currently, he is head of a research group which is involved in activities in the field of high frequency measuring and sensor systems, antennas based on three dimensional molded interconnect device technology (3D MID) and future radio frequency identification (RFID) systems.

Dr. Geck is cofounder of Triovacos GmbH (2011). Triovacos offers products and services in the areas of RFID and Near Field Communication (NFC).